Polarized infrared reflectivity study of an oriented ceramic of $Bi_2Sr_2Ca_2Cu_3O_{10+\delta}$ (Bi-2223)

N. Petit[1], V. Garnier[2], V. Ta Phuoc[1], R. Caillard[2], A.-M. Frelin[1], A. Ruyter[1], I. Laffez[1], J.-C. Soret[1], A. Maignan[2], and F. Gervais[1,a]

[1] Laboratory of electrodynamics of advanced materials, LRC M01 associated to CEA, FRE 2077 associated to CNRS, François Rabelais University, 37200 Tours, France

[2] CRISMAT[b], ISMRA, boulevard Maréchal Juin, 14050 Caen, France

Abstract. The reflectivity spectra of an oriented ceramic of Bi-2223 has been investigated by polarized infrared reflectivity spectroscopy in the energy range 0.005–2.2 eV. It is shown that the data for the polarization parallel to the c axis cannot be fitted with a one-component Drude or extended-Drude model. The conductivity spectrum is then obtained from the best fit of a "double-damping Drude" model to reflectivity spectra, itself derived from the factorized form of the dielectric function, and by a Kramers-Kronig inversion as well. The data and their analysis give a new insight of the 2D character of the system.

PACS. 71.38.-k Polarons and electron-phonon interactions – 63.20.Kr Phonon-electron and phonon-phonon interactions – 78.20.Ci Optical constants (including refractive index, complex dielectric constant, absorption, reflection and transmission coefficients, emissivity)

1 Introduction

Among oxides of transition metal elements showing prominent properties, high-T_c cuprate materials are the subjects of considerable interest. Even fifteen years after the discovery by Bednorz and Müller [1], they still raise the unsolved problem of the intimate origin of the phenomenon. In the meantime, most technological potential applications require the alignment of the (ab) planes. There is a consensus to recognize that the bidimensionality of the structure is key point of the property itself. This is the reason why elaboration methods able to preserve the 2D orientation appear of formidable technological interest. Apart from single crystal growth, those methods are either epitaxial growth by various deposition techniques, or texturation of ceramics. This is the last one that is exploited here. On the other hand, few cuprate compositions give rise to superconductivity up to critical temperature reaching or exceeding 110 K. Only certain bismuth, lead, thallium or mercury compounds enter this category. Three of them contain toxic elements, favoring bismuth compounds for promising technological applications. Bismuth compounds single crystals preferentially grow in thin film shape parallel the (ab) plane. Available thickness along the c axis did not exceed a fraction of millimeter up to now. The smallness of this dimension has prevented generalized optical and infrared measurements polarized par-

allel to the c axis. In the family of high-T_c cuprate superconductors, most investigated samples for the polarization parallel to the c axis are $La_{2-x}Sr_xCuO_{4-\delta}$ (LSCO) and related compounds with various substitutions [2–5] $YBa_2Cu_3O_{7-\delta}$(YBCO) [6–13] and Bi or Tl-based compounds with single or double CuO_2 planes, noted 2201 or 2212, respectively [14–17]. A charge carrier signature is observed parallel to the c axis in YBCO in the normal phase plus an additional contribution in the superconducting phase, both of them highly coupled with the phonon contributions [7,8]. LSCO and Tl and Bi-based cuprates (in particular with a single cuprate layer) rather show a low-frequency feature in the superconducting phase assigned to Josephson effect [2,4,12,13,15–18]. The purpose of this paper is at least twofold: (i) to report infrared reflectivity spectra of a sample of Bi-2223, in particular for the polarization parallel to the c axis for which there is an important lack of data in the literature, (ii) beyond this specific case, to analyze the data in terms of optical conductivity by both Kramers-Kronig inversion and fitting with a model appropriate for both polarizations parallel and perpendicular to the c axis.

2 Experiments

- Sample preparation and preliminary characterization

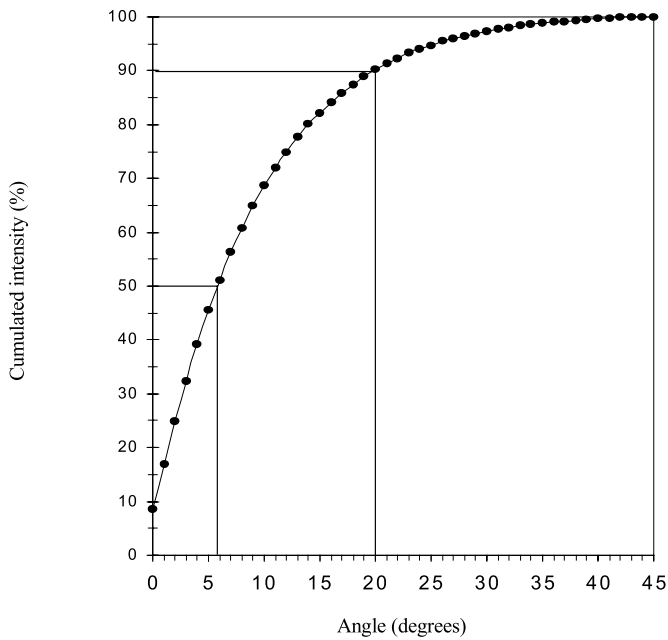Using the nominal composition $Bi_{1.85}Pb_{0.35}Sr_2Ca_2Cu_{3.1}O_{10+y}$, suggested by Maeda [19] and adopted by many other

---

Fig. 1. Cumulative X-ray intensity curve of the Bi-2223 sample showing that 50% of the grains are aligned within 6°.

Fig. 2. SEM micrographs of the Bi-2223 sample – A: secondary phases and porosity – B: good overall grain alignment – C: example of local misalignment induced by the presence of non-superconducting phase.

groups [20–22], the powder precursor was obtained by the polymer matrix method as described elsewhere starting from the corresponding metal acetates [23]. Then, after milling, the powder was calcined at 820 °C for 24 hours. This powder is mainly composed of 2212, Ca_2PbO_4, Ca_2CuO_3 and CuO phases, necessary for the 2223 phase formation during sintering. The resulting powder is milled again and pelletized (3 g, 16 mm diameter, 1.5 ton/cm^2) to be sintered. Several sintering steps with intermediates milling are necessary to form up to 95% of 2223 phase. This estimation has been done with Schmahl program [24] which enable us to take into account the area of several diffraction peaks of the 2201, 2212 and 2223 phases with their relative intensity and the preferential orientation phenomena. The resulting sintered pellets are then sinter-forged [25] one a time at 820 °C for 20 hours under 20 MPa to obtain dense textured ceramic disks ($\approx$ 1 mm thickness). Height of those disks are piled to be link together by an additional short sinter-forging step (4 hours at 810 °C under 7 MPa). Thick 2223 ceramic is obtained (up to 5 mm). The (0 0 <u>10</u>) pole figure measurement was performed on this bulk sample (Fig. 1) with a Philips X'Pert X-ray diffractometer and revealed that 50% of the total amount of the 2223 grains are aligned within an angle of 6°. SEM observation (Fig. 2A) shows a large 2223 matrix (gray) with some brighter and darker residual phases (SrCaCuO) [26]. Some dark areas may also correspond to porosity. Density measurements have revealed up to 92% of densification. The sample microstructure (Fig. 2B) exhibits good 2223 grain alignment. However, some local misalignment in the texture are observed (Fig. 2C), induced by the presence of non-superconducting residual phase grains whose shape is almost isotropic and size larger than the thickness of the 2223 platelet grains. Mag-
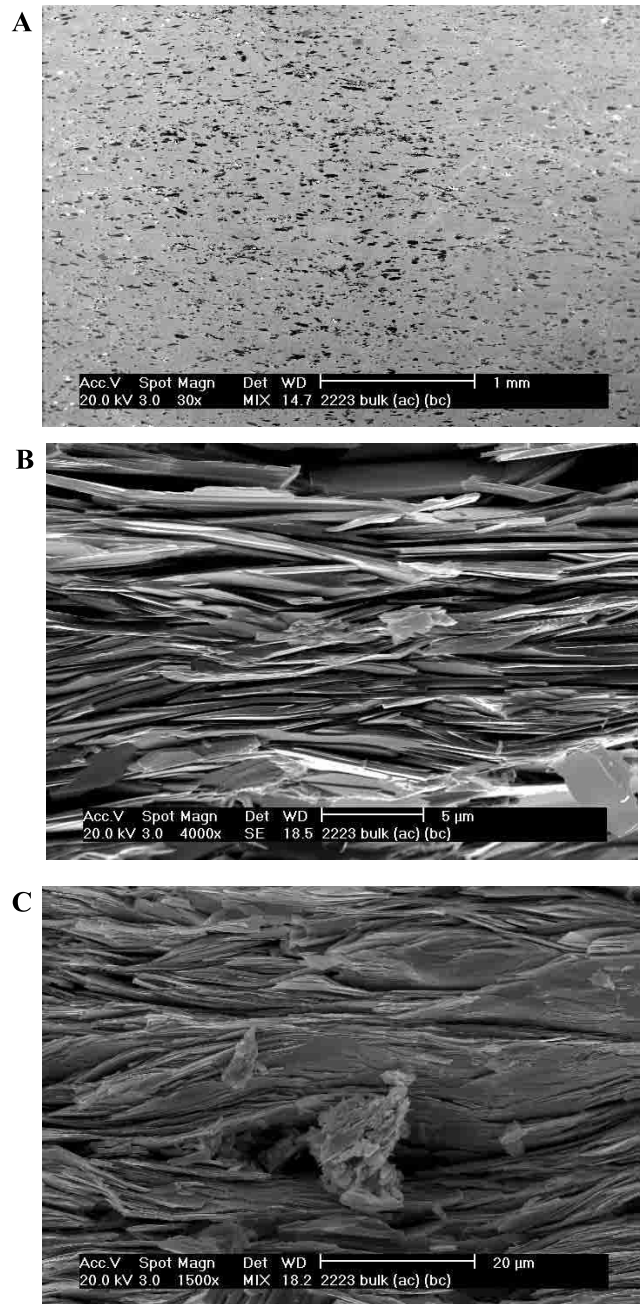
netization measurements have been performed on the Bi-2223 bulk sample (Fig. 3). The transition is quite broad and the T_c onset is about 104–105 K. Thermoelectric power measurements (Fig. 4) have also been performed as a function of temperature and have shown that at 290 K the TEP is $\sim +11$ μv K^{-1}. According to the results of Obertelli *et al.* [27], this value indicates an underdoped state which yields $T_c = 104-105$ K ($T_{c\ max}$(Bi-2223) = 110 K). This T_c value is in agreement with the T_c deduced from the magnetization measurements shown in
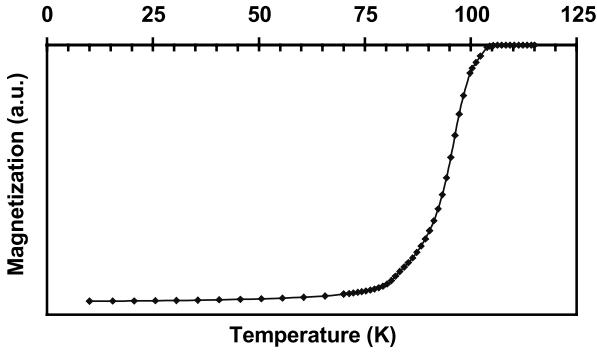
Fig. 3. Temperature dependence of magnetization showing the onset of superconductivity at 104–105 K in the Bi-2223 sample.
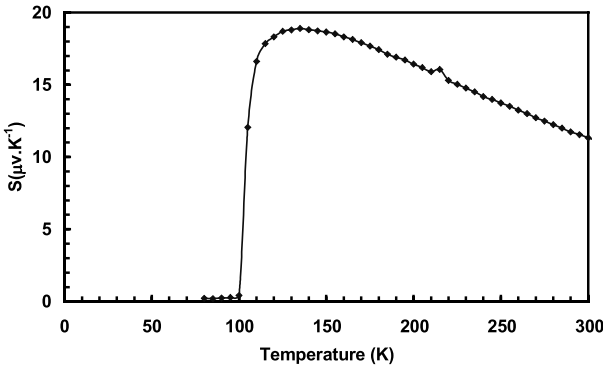

Fig. 4. Temperature dependence of thermoelectric power of the sample.

Fig. 5. Reflectivity spectra of the oriented ceramic sample of Bi-2223 measured with a polarized radiation along the **c** axis (lower spectrum) and the $(\mathbf{a}, \mathbf{b})$ plane (upper spectrum). The dotted line represents the best fit of the spectra in each case, using the double damping Drude model equation (9). The residues of the phonons of the other polarization due to the imperfect alignment of the crystallites were not fitted in the upper spectrum.

Figure 3, *i.e.* 5 K below the optimum for this as-prepared phase that thus appears slightly underdoped.

- Reflectivity measurements

The infrared reflectivity spectra of the Bi-2223 textured sample have been measured with a Bruker IFS 66v/S in the wave number range 40–18,000 cm^{-1} (5 meV–2.2 eV). For the far-infrared region, the polarization of the radiation was obtained *via* a polarizer on polyethylene window, and for the mid-infrared with a KRS5 one. The sample was cut parallel to the c axis and then polished. The alignment inside the spectrometer was made by rotating the direction of polarization and by searching for the maxima and minima of reflected signal, assigned to the direction perpendicular and parallel to the c axis, respectively. The angle between both orientations that were found, was checked to be 90°. Figure 5 shows the spectra obtained for both directions of polarization. The residual small bumps below 0.1 eV for the polarization perpendicular to the c axis are likely related to phonons active in the other polarization due to the imperfect orientation of the sample. Ignoring this effect, the level of reflectivity and the profile of the spectrum obtained in the present work for the (a, b) plane compares well with data obtained by reflectivity measurements upon thin films [28–30]. On the other hand, the spectrum for the polarization parallel to the c axis is original to the best of our knowledge, for lack of single crystal
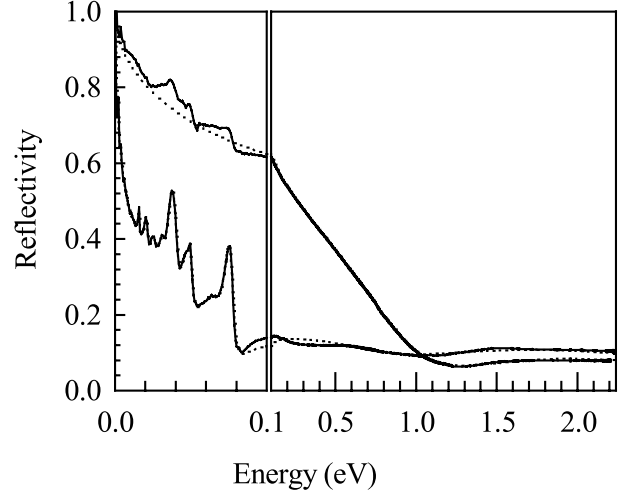
thick enough in the c axis direction. The results show sufficiently high anisotropy to allow further analysis.

3 Optical conductivity

The optical conductivity has been deduced from the reflectivity spectra by means of two methods. Kramers-Kronig (KK) inversion has been performed in a first step. The KK transformation allows the calculation of the phase angle from the reflectivity spectrum $R(\omega)$ *via*

$$\theta(\omega') = -\frac{1}{2\pi} \int_0^\infty \ln \left(\frac{\omega + \omega'}{|\omega - \omega'|} \right) \frac{\mathrm{d} \ln R(\omega)}{\mathrm{d}\omega} \mathrm{d}\omega \quad (1)$$

which allows the determination of all optical functions such as the complex refractive index $\widetilde{n}(\omega)$

$$\widetilde{n}(\omega) = \eta(\omega) - \mathrm{i}\kappa(\omega) \quad (2)$$

via

$$\eta(\omega) = \frac{1 - R(\omega)}{1 - 2\sqrt{R(\omega)} \cos \theta(\omega) + R(\omega)} \quad (3)$$

$$\kappa(\omega) = \frac{2\sqrt{R(\omega)} \sin \theta(\omega)}{1 - 2\sqrt{R(\omega)} \cos \theta(\omega) + R(\omega)} . \quad (4)$$

As well as the dielectric response $\widetilde{\varepsilon}(\omega)$

$$\widetilde{\varepsilon}(\omega) = \widetilde{n}^2(\omega). \quad (5)$$

The conductivity spectrum $\widetilde{\sigma}(\omega)$ is then deduced *via*:

$$\widetilde{\varepsilon}(\omega) = \varepsilon_\infty - \frac{\mathrm{i}\widetilde{\sigma}(\omega)}{\varepsilon_v \omega} . \quad (6)$$
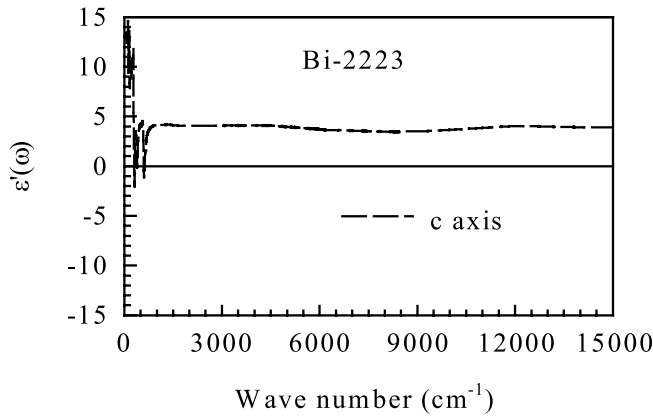
Fig. 6. Real part of the dielectric response deduced from a Kramers-Kronig (KK) inversion of reflectivity spectra for the polarization parallel to the c axis. ε' is found positive at nearly all frequencies, contrary to the expectations of the Drude model, and equal or larger than ε_∞ at most frequencies.

Where ε_∞ is the "high-frequency" dielectric constant, in practice corresponding to an energy just below the optical gap energy.

Reported attempts to fit the reflectivity spectra of cuprates are seldom. Authors generally perform Kramers-Kronig inversion and discuss the spectral weight and its evolution with temperature and frequency. To the best of our knowledge, the only systematic fitting analysis for the polarization parallel to the c-axis of a cuprate, posterior to the works of our group [7,8], is reported in reference [31]. But charge-carrier fitting parameters are not reported. Present attempts to fit the c-axis reflectivity spectrum with the conventional Drude model failed, consistent with previous studies of YBCO [7,8]. Attemps to derive a plasmon damping function as usually done in "extended" version of the Drude model

$$\widetilde{\varepsilon}(\omega) = \varepsilon_\infty \left[1 - \frac{\Omega_{\mathrm{P}}^2}{\omega(\omega - \mathrm{i}\gamma(\omega))} \right] \qquad (7)$$

also failed. The damping function evaluated from the dielectric response deduced from the KK analysis

$$\gamma(\omega) = \frac{\omega \varepsilon''(\omega)}{\varepsilon_\infty - \varepsilon'(\omega)} \qquad (8)$$

indeed is negative or anomalously high in certain frequency ranges because the condition $\varepsilon'(\omega) < \varepsilon_\infty \forall \omega$ is not obeyed, contrary to conventional metals. The real part of dielectric response remains positive nearly everywhere (Fig. 6), whereas in conventional metals, ε' becomes negative below the plasma frequency. Figure 7 that displays the conductivity calculated *via* KK transformation shows that, contrary to the prediction of the Drude model, the conductivity is not maximum at zero frequency. This is particularly true for the c-axis polarization.

Since none one-component model appears applicable for the c-axis direction, we tried a two-component model. The one retained after several unfruitful tests is derived
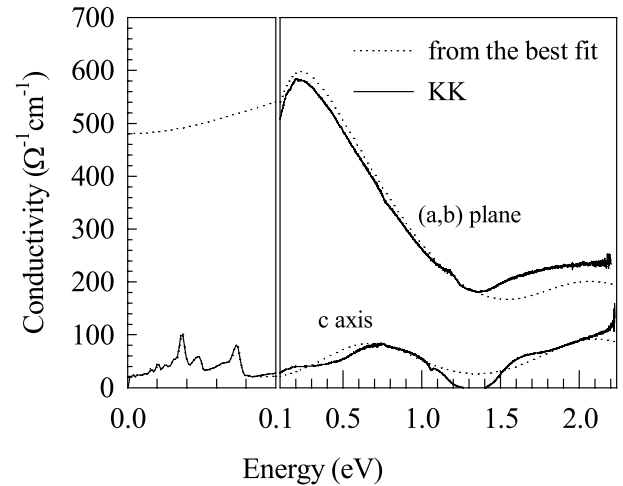

Fig. 7. Real part of the conductivity obtained from the polarized reflectivity spectra of Bi-2223 deduced both by a Kramers-Kronig (KK) transformation (continuous line) and from the best fit (dotted line). For the sake of clarity, the low-frequency experimental data are omitted for the basal plane, because they mistakenly amplify the residues of the phonons of the other polarization related to the imperfect alignment of the crystallites.

from a factorized form of the dielectric function [32,33]. In this model, the dielectric function is written as

$$\widetilde{\varepsilon}(\omega) = \varepsilon_\infty \left[\prod_j \frac{\Omega_{j\mathrm{LO}}^2 - \omega^2 + \mathrm{i}\gamma_{j\mathrm{LO}}\omega}{\Omega_{j\mathrm{TO}}^2 - \omega^2 + \mathrm{i}\gamma_{j\mathrm{TO}}\omega} - \frac{\Omega_{\mathrm{P}}^2 + \mathrm{i}(\gamma_{\mathrm{P}} - \gamma_0)\omega}{\omega(\omega - \mathrm{i}\gamma_0)} \right] \qquad (9)$$

where the first part of the right-hand side is inherited from the generalized Lyddanne-Sachs-Teller relationship and describes oscillatory contributions (such as phonons, trapped polarons, and all oscillations implying a restoring force). The second one concerns oscillations without restoring force such as free carriers here expressed *via* a plasma-like contribution with Ω_{P} the plasma frequency defined *via*

$$\Omega_{\mathrm{P}}^2 = \frac{ne^2}{m^* \varepsilon_v \varepsilon_\infty} \qquad (10)$$

inherited from the Drude model. γ_{P} represents the linewidth of the plasma response centered at $\omega = \Omega_{\mathrm{P}}$ and γ_0 the linewidth of the free-carrier absorption centered at $\omega = 0$. The usual Drude model is recovered on setting $\gamma_0 = \gamma_{\mathrm{P}}$. The reflectivity is calculated *via* the Fresnel formula near normal incidence

$$R(\omega) = \left| \left(\sqrt{\widetilde{\varepsilon}(\omega)} - 1 \right) \Big/ \left(\sqrt{\widetilde{\varepsilon}(\omega)} + 1 \right) \right|^2 \qquad (11)$$

and the spectral conductivity $\widetilde{\sigma}(\omega)$ *via* (6). The best fit of equations (9, 11) to reflectivity data is shown in Figure 5. Fitting parameters are given in Table 1. Note that since γ_{P} is equal to γ_0 for the (*ab*) plane, a conventional Drude contribution would fit the data equally well (added to a

Table 1. Parameters which yields the best fit of equation (9) to experimental spectra. $\varepsilon_\infty = 4$ for both polarizations.

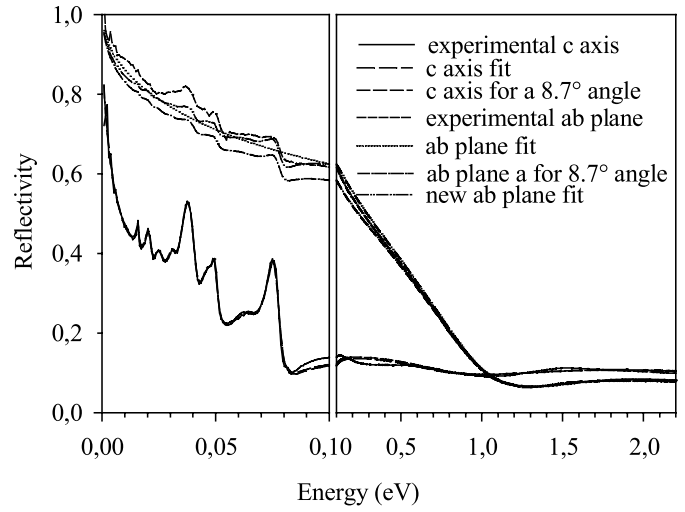| Ω_{TO}	γ_{TO}	Ω_{LO}	γ_{LO}
(ab)-plane polarization			
3862	10900	8222	7650
16305	12200	18000	13400
Ω_{P}	γ_{P}	γ_0	
4000	2200	2200	
c axis polarization			
Ω_{TO}	γ_{TO}	Ω_{LO}	γ_{LO}
127	8.9	130	8.7
165	19	171	17
205	32	211	31
252	31	256	29
298	39	334	27
368	46	385	45
397	22	410	17
510	101	528	96
599	44	633	4.5
6820	8900	7163	7400
17175	10700	17890	10600
Ω_{P}	γ_{P}	γ_0	
200	520	120	

Fig. 8. Comparison of spectra calculated with a 8.7° average misalignment of crystallites with respect to c-axis and (ab) plane, with experimental spectra. It is seen that the c-axis spectrum remains practically unchanged while the signature of c-axis phonons is compatible with the experimental (ab) plane. "New fit (ab) plane" refers to the spectrum obtained by increasing the plasma frequency by 5% (and decreasing plasma dampings by 20%) to recover the experimental spectrum.

broad oscillator in the mid infrared). But this is no longer true for the c-axis spectrum.

Since a signature of leakage of c-axis polarized phonons is observed in the (ab) plane spectrum, we have an additional optical way to test the effect of misalignment of crystallites. Reference [11] suggests taking account of the effect of leakage with the simple formula

$$R = (1 - z)R_{\text{c}} + zR_{\text{ab}}. \tag{12}$$

If we do so and then Kramers-Kronig transform the reflectivity spectra, a bump appears in the conductivity spectra at frequencies compatible with those observed in Figure 7 and one may therefore wonder if observed bumps would not be due to the spurious effect of polarization leakages. Note however that a bump at 1000 cm^{-1} was added to fit the data of a thin film of Bi-2223 in reference [30]. Formula (12) actually assumes a kind of twinned crystal with a percentage of crystallites aligned perpendicular to the direction of polarization and infrared active nevertheless. Figures 1 and 2 definitely show this is not the situation in our sample. If the direction of polarization of the electromagnetic radiation makes an angle θ with the c-axis of a crystallite, the dielectric response actually is given by

$$\frac{1}{\varepsilon(\vartheta)} = \frac{\cos^2\theta}{\varepsilon_{\text{c}}} + \frac{\sin^2\theta}{\varepsilon_{\text{(ab)}}} . \tag{13}$$

Figure 8 shows that the calculation based on $\varepsilon_{\text{(ab)}}$ and ε_{c} determined by the fitting procedure of the previous step with an average angle of 8.7°, fits almost exactly the profile of the experimental (ab)-plane spectrum. *A profile almost indistinguishable is obtained by using the data of Figure 1 and by integrating over all misalignment angles* (Fig. 8). In both cases, the reflectivity level, however, is slightly lowered with respect to the experiment. To compensate, the new "best fit" for the (ab) plane assumes a plasma frequency increased by 5% and plasma dampings decreased by 20% with respect to the data of Table 1. Conversely, for the c-axis polarization, Figure 8 shows that the same 8.7° average misalignment gives a spectrum practically indistinguishable from the 0° spectrum. For the c-axis polarization, an angle θ larger than 20° in equation (12) is required to observe a spectrum that differs from the experiment by a quantity larger than the experimental uncertainty. Since the most original point of the present paper just concerns the c-axis spectrum, we may, therefore, further analyze and exploit the spectrum and the parameters obtained, neglecting crystallite misalignment.

Figure 7 shows the real part of the optical conductivity. The unbroken line represents the result of a Kramers-Kronig transformation performed in the whole measurement range (not plotted in the phonon leakage region for the (ab) polarization to avoid confusion). The dotted line is calculated from the parameters that yield the best fit with the double damping Drude model equation (9). For each polarization direction, the agreement of the KK conductivity and that obtained from the best fit is satisfactory. In addition to various conducting oxides [32,33], including cuprates [7,8] the phenomenological model equation (9) has been recently successfully applied

to manganites [34] and even to conducting polymers [35]. The satisfactory fitting in the present case is therefore not surprising. Figure 9 illustrates the contribution of mobile charge carriers to the total conductivity. This is an additional advantage of the fitting procedure that allows the discrimination of mobile (without restoring force) and trapped charged species (such as phonons or trapped polarons). Note in the figure that the mobile charge carriers consistently are responsible alone for the zero frequency (DC) conductivity. The bump in the-mid infrared, well visible for the polarization parallel to the c axis but also necessary to fit the spectrum of the (ab) plane, consistent with reference [30], is attributed to trapped polarons [36,37]. An optimal doping of Bi-2223 is expected for 0.16 hole per copper atom of the (a, b) plane [38], *viz.* 8.8×10^{20} hole/cm^3. Since the model allows discriminating the part of the conductivity corresponding to excitations with and without restoring forces, it is easy to integrate the area under the sole contribution of mobile charge carriers to the optical conductivity to deduce a number of mobile carriers weighted by the carrier effective mass

$$\int_0^{\omega_c} \sigma(\omega')\mathrm{d}\omega' = \frac{\pi e^2}{2} \frac{N_{\mathrm{eff}}(\omega)}{m^*} . \tag{12}$$

On taking $\omega_c = 1.1$ eV (the contribution becomes low and inaccurate above) and assuming the electron mass for the carriers, one finds 6×10^{20} hole/cm^3, consistent with the slightly underdoped character of the sample, discussed in Section 2. For the polarization parallel to the c axis, $N_{\mathrm{eff}}(1.1$ eV$)$ is found much lower, only 10^{20} hole/cm^3. The contribution of trapped carriers, $N_{\mathrm{eff}}(1.1$ eV$) = 1.1 \times 10^{21}$ carriers/cm^3 for the polarization within the basal plane is found larger than that of mobile carriers for this polarization and concentrated in the bump near 0.7 eV. These data confirm the analysis of the real part of the dielectric response shown in Figure 8 pointing towards the need for a two-component model to describe the response of underdoped Bi-2223 sample, a view that appears compatible with polaronic scenarios [36,37].

Phonon parameters for the polarization parallel to the c axis (Tab. 1) may be compared with data of references [31,39] deduced for the same polarization from grazing incidence reflectivity measurements. The set of data that, in principle, should be the closest to the present data concerns $Tl_2Ba_2Ca_2Cu_3O_{10}$ with three consecutive conductive CuO_2 planes. Spectra of reference [39] unfortunately were not fitted. No clear correspondence of conductivities emerges although both compounds share similar blocks in their respective structures. Actually, apart from the O-O vibration at the highest TO frequency (near 600 cm^{-1}), that is common to all spectra, no obvious correspondence can be safely established in other Tl-based or Bi-based compounds. The strongest mode lies at 298 cm^{-1} in Bi-2223, 20-30% lower than the strongest mode observed in 2212 or 2201 and assigned in reference [31] to Cu-O vibration. Lattice dynamical calculations for this structure would be needed to allow assignments.
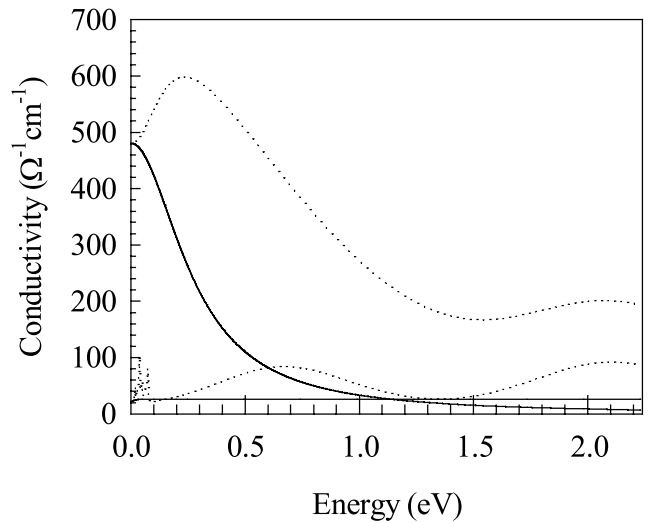

Fig. 9. Contribution of the sole mobile carriers (continuous lines) to the total conductivity (dotted lines) for both polarizations. Upper part: (a,b) plane. Lower part: c axis.

4 Conclusion

A thick ceramic of Bi-2223 with 50% of the grains aligned within an angle of 6° has been investigated by infrared-visible reflectivity measurements. The reflectivity in the ab plane has already been measured in Bi-2223 thin films but to the best of our knowledge not along the c axis, because the growth of sufficiently thick single crystal sample has failed up to now. Despite the error induced by the aforementioned misalignment, the reflectivity spectrum along the c axis shows considerable difference from that for the (ab) plane. The leakage of the phonon c axis spectrum apparent in the (ab)-plane spectrum was fitted with an angle-dependent dielectric function model that, conversely applied to the other polarization, shows that the effect of the crystalline misalignment upon the reflectivity is negligible for the c-axis polarization. It is shown that no single-component model, Drude or extended-Drude, is able to fit the c-axis data. The optical conductivity has been studied and parameterized in the framework of the double damping Drude model inherited from the factorized form of the dielectric response, little exploited in the recent cuprate literature [13,40]. The concentration of mobile charge carriers is consistent with that expected for an underdoped sample for the (a, b) plane. The anisotropy of the optical conductivity extrapolated to zero frequency reaches a factor of 25, consistent with the bi-dimensional character of the system showing, *via* this result, the essential preservation of the 2D properties thanks to the texturation process. The confirmation of present results in a single crystal sample is highly desirable. Recent literature [4,5,10–15,17,18] indeed focus on the analysis of c-axis data to help understanding the origin of high-T_c superconductivity in cuprates.

References

1. J.G. Bednorz, K.A. Müller, Z. Phys. B **64**, 189 (1986).
2. S. Uchida, K. Tamasaku, S. Tajima, Phys. Rev. B **53**, 14558 (1996).
3. T. Startseva *et al.*, Phys. Rev. B **59**, 7184 (1999).
4. Y. Fukuzumi, K. Mizuashi, S. Uchida, Phys. Rev. B **61**, 627 (2000).
5. S. Tajima, T. Noda, H. Eisaki, S. Uchida, Phys. Rev. Lett. **86**, 500 (2001).
6. Homes, T. Timusk, D.A. Bonn, R.A. Liang, W.N. Hardy, Physica C **254**, 265 (1995).
7. R.P.M.S. Lobo, F.J. Gotor, P. Odier, F. Gervais, Phys. Rev. B **53**, 410 (1996).
8. F. Gervais, R.P.M.S. Lobo, Z. Phys. B **104**, 681 (1997).
9. V. Puchkov, D.N. Basov, T. Timusk, J. Phys. Cond. Matt. **8**, 10049 (1996).
10. C. Bernhard, R. Henn, A. Wittlin, M. Kläser, Th, Wolf, G. Müller-Vogt, C.T. Lin, M. Cardona, Phys. Rev. Lett. **80**, 1762 (1998).
11. D.N. Basov, C.C. Homes, E.J. Singley, M. Strongin, T. Timusk, G. Blumberg, D. Van der Marel, Phys. Rev. B **63**, 134514 (2001).
12. H. Shibata, T. Yamada, Phys. Rev. Lett. **81**, 3519 (1998).
13. T. Kakeshita, S. Uchida, K.M. Kojima, S. Adachi, S. Tajima, B. Gorshunov, M. Dressel, Phys. Rev. Lett. **86**, 4140 (2001).
14. A.S. Katz, S.I. Woods, E.J. Singley, T.W. Li, M. Xu, D.G. Hinks, R.C. Dynes, D.N. Basov, Phys. Rev. B **61**, 5930 (2000).
15. T. Motohashi, J. Shimoyama, K. Kitazawa, K. Kishio, K.M. Kojima, S. Ushida, S. Tajima, Phys. Rev. B **61**, R9269 (2000).
16. V. Zelezny, S. Tajima, D. Munzar, T. Motohashi, J. Shimoyama, K. Kishio, Phys. Rev. B **63**, 60502 (2001).
17. D. Munzar, C. Bernhard, T. Holden, A. Golnik, J. Humlicek, M. Cardona, Phys. Rev. B **64**, 24523 (2001).
18. D. Dulic *et al.*, Phys. Rev. Lett. **86**, 4144 (2001).
19. Maeda, K. Noda, K. Uchinokura, S. Tanaka, Jpn J. Appl. Phys. **28**, L576 (1989).
20. S. Hong, T.O. Mason, C.K. Chiang, S.W. Freiman, N.M. Huang, Appl. Supercond. **1**, 109 (1993).
21. U. Endo, S. Kayama, T. Kawai, Jpn J. Appl. Phys. **27**, L1476 (1988).
22. Wang, M. Wakata, T. Kaneko, S. Takano, H. Yamauchi, Physica C **208**, 323 (1993).
23. V. Garnier, I. Monot-Laffez, G. Desgardin, Supercond. Sci. Technol. **13**, 602 (2000).
24. W.W. Schmahl, M. Lehmann, S. Räth, M. Gerards, R. Riddle, Supercond. Sci. Technol. **11**, 1269 (1998).
25. R. Caillard, V. Garnier, G. Desgardin, Physica C **340**, 101 (2000).
26. V. Rouessac, G. Poullain, G. Desgardin, Supercond. Sci. Technol. **11**, 1160 (1998).
27. S.D. Obertelli, J.R. Cooper, J.L. Tallon, Phys. Rev. B **46**, 14928 (1992).
28. E.A. Kafadaryan, M.V. Simonyan, S.Ph. Pilosyan, R.B. Akopyan, V.T. Tatoyan, Supercond. Phys. Chem. Technol. **4,** 1334 (1991).
29. P. Calvani, M. Capizzi, P. Dore, S. Lupi, P. Maselli, G. Paleologo, G. Balestrino, M. Marinelli, E. Milani, H. Berger, P. Roy, Y.L. Mathis, Int. J. Infrared MM. Waves **14**, 251 (1993).
30. A. El Azrak, R. Nahoum, N. Bontemps, M. Guilloux-Viry, C. Thivet, A. Perrin, S. Labdi, H. Raffy, Phys. Rev. B **49**, 9846 (1994).
31. A.A. Tsvetkov *et al.*, Phys. Rev. B **60**, 13196 (1999).
32. F. Gervais, in *Infrared and millimeter waves*, Vol. 8 (Academic Press, 1983).
33. F. Gervais, J.L. Servoin, A. Baratoff, J.G. Bednorz, G. Binnig, Phys. Rev. B **47**, 8187 (1993).
34. N. Petit, C. Daulan, J.C. Soret, A. Maignan, F. Gervais, Eur. Phys. J. B **14**, 617 (2000).
35. N. Petit, F. Gervais, P. Buvat, P. Hourquebie, P. Topart, Eur. Phys. J. B **12**, 367 (1999).
36. D.M. Eagles, R.P.S.M. Lobo, F. Gervais, Phys. Rev. B **52**, 6440 (1995).
37. S. Lupi, P. Maselli, M. Capizzi, P. Calvani, P. Giura, P. Roy, Phys. Rev. Lett. **83**, 4852 (1999).
38. M.R. Presland, J.L. Tallon, R.G. Buckley, R.S. Liu, N.E. Flower, Physica C **176**, 95 (1991).
39. J.H. Kim, B.J. Feenstra, H.S. Somal, D. Van der Marel, W.Y. Lee, A.M. Gerrits, A. Wittlin, Phys. Rev. B **49**, 13065 (1994).
40. Z.V. Popovic, M.J. Konstantinovic, V.A. Ivanov, O.P. Khuong, R. Gajic, A. Vietkin, V.V. Moshxhalkov, Phys. Rev. B **62**, 4963 (2000).